Critical slowing down in purely elastic 'snap-through' instabilities

Michael Gomez, Derek E. Moulton and Dominic Vella*
Mathematical Institute, University of Oxford, Woodstock Rd, Oxford, OX2 6GG, UK

Many elastic structures have two possible equilibrium states [1]: from umbrellas that become inverted in a sudden gust of wind, to nano-electromechanical switches [2, 3], origami patterns [4, 5] and the hopper popper, which jumps after being turned inside-out [6]. These systems typically transition from one state to the other via a rapid 'snap-through'. Snap-through allows plants to gradually store elastic energy, before releasing it suddenly to generate rapid motions [7, 8], as in the Venus flytrap [9]. Similarly, the beak of the hummingbird snaps through to catch insects mid-flight [10], while technological applications are increasingly exploiting snap-through instabilities [11–13]. In all of these scenarios, it is the ability to repeatedly generate fast motions that gives snap-through its utility. However, estimates of the speed of snap-through suggest that it should occur more quickly than is usually observed. Here, we study the dynamics of snap-through in detail, showing that, even without dissipation, the dynamics slow down close to the snap-through transition. This is reminiscent of the slowing down observed in critical phenomena, and provides a handheld demonstration of such phenomena, as well as a new tool for tuning dynamic responses in applications of elastic bistability.

Snap-through occurs when a system is in an equilibrium state that either ceases to exist or becomes unstable as a control parameter varies: the system must jump to another equilibrium state. For example, in the Venus flytrap it is believed that the natural curvature of the leaf changes slightly making the 'open' equilibrium disappear leaving only the 'closed' equilibrium [9].

Bistability and snap-through can be demonstrated using an elastic strip of length L whose edges are clamped at equal angles $\alpha \neq 0$ to the horizontal (Fig. 1a) [14, 15]. Provided that the two ends of this arch are brought together by a large enough distance ΔL, two stable shapes exist: the 'natural' mode and an 'inverted' shape (Fig. 1a). However, as ΔL is gradually decreased (pulling the two ends apart), the inverted equilibrium shape suddenly snaps through to the natural shape. The bifurcation diagram for this system (Fig. 1a) shows that as ΔL is decreased the inverted state becomes unstable, before ceasing to exist at still smaller ΔL.

Snap-through due to an equilibrium state becoming unstable, as in the above example, is generally amenable to linear stability analysis [6, 16]: the displacement of each point on the arch evolves in time as $\sim e^{\sigma t}$ for some growth rate σ. The more dynamically interesting snap-through occurs when an equilibrium state ceases to exist without first becoming unstable (known as a saddle-node/fold bifurcation or limit-point instability [17]). This textbook snap-through [1] can be obtained simply by holding one end of the strip horizontally, while the other remains clamped at the angle α (Fig. 1b).

The change in bifurcation to a saddle-node type means that a standard linear stability analysis no longer applies. Many previous works adopt a purely numerical approach to study the dynamics in this scenario [14]. In a simple elastic model, transverse displacements $w(x,t)$ of the strip are governed by the dynamic beam equation:

$$\rho_s h \frac{\partial^2 w}{\partial t^2} + B\frac{\partial^4 w}{\partial x^4} + P\frac{\partial^2 w}{\partial x^2} = 0, \qquad 0 < x < L, \quad (1)$$

with the material properties of the strip denoted by ρ_s (density), h (thickness) and $B = Eh^3/12$ (bending stiffness, with E the Young's modulus); P is the applied compressive load (per unit width). An alternative approach is to estimate the time scale of snapping by balancing the first two terms in (1), suggesting that snap-through should occur on a time scale

$$t_* = \left(\frac{\rho_s h L^4}{B}\right)^{1/2} \sim \frac{L^2}{h\sqrt{E/\rho_s}}. \quad (2)$$

This time scale involves the speed of sound within the strip, $(E/\rho_s)^{1/2}$, and so is typically very short. However, the above estimate frequently overestimates the speed of snapping, with the discrepancy attributed to some form of dissipation [9, 14]. We investigate this snap-through 'bottleneck' using a controlled version of our handheld snapping experiment and detailed analysis of (1) .

We performed experiments on thin strips of polyethylene terephthalate (PET) and stainless steel shim (see Methods). A strip is clamped (with ends angled appropriately) and then buckled into an arch by imposing an end-shortening ΔL (Fig. 2a). Snap-through is reached by altering ΔL quasi-statically to values $\Delta L < \Delta L_{\text{fold}}$, with the threshold ΔL_{fold} determined experimentally (see Supplementary Information for details). To obtain repeatable experiments with a given value of $\Delta L < \Delta L_{\text{fold}}$, the strip is initially prevented from snapping by an indenter that fixes the displacement of the midpoint to be that at the bifurcation point, $w_{\text{fold}}(L/2)$. On removing the constraint, the strip then snaps from rest (Fig. 2b, Supplementary Movie 1).

A spatio-temporal plot of the midpoint position during snap-through (Fig. 2c) reveals the nonlinear nature of

* dominic.vella@maths.ox.ac.uk

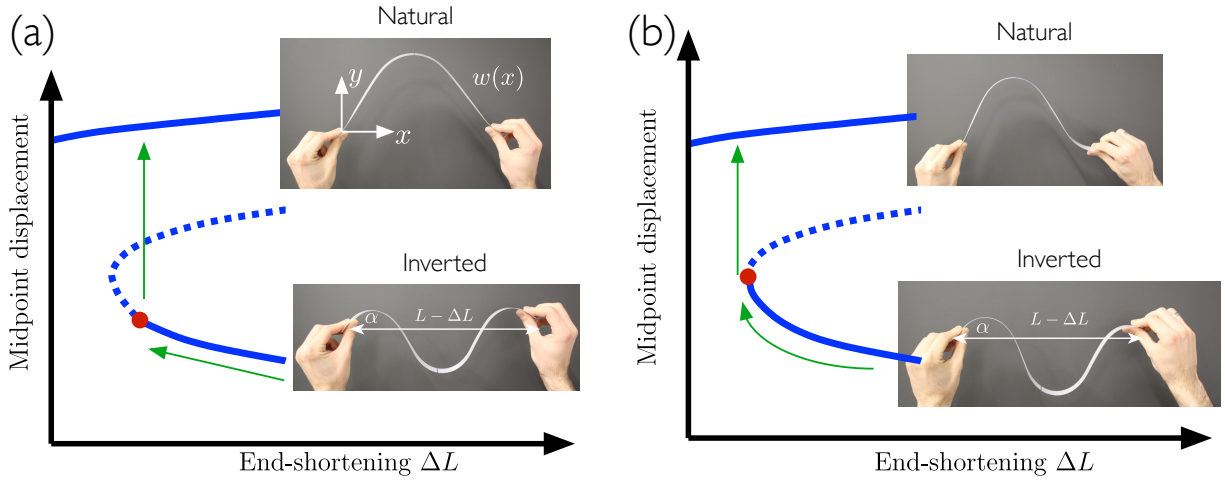

FIG. 1. Exploring 'snap-through' instabilities in a simple elastic system. (a) Bringing the edges of a strip of plastic together, while also holding them at a non-zero angle α to the horizontal, creates bistable 'inverted' (bottom) and 'natural' (top) arch shapes. Under smaller end-shortenings ΔL, the arch snaps from the inverted to the natural shape. Analysing the bifurcation behaviour shows that the instability underlying snapping in this case is a subcritical pitchfork bifurcation: the inverted mode (lower solid curve) intersects an unstable asymmetric mode (not drawn) at the point marked with a red dot; here it becomes linearly unstable (dashed curve). (Because the asymmetric mode is unstable it is not observed in practice.) (b) Introducing asymmetry in the boundary conditions, by holding the right end horizontally, still creates a bistable system. However, the destabilizing effect of the asymmetric mode is removed and the inverted mode remains stable up to a fold (indicated by the red dot): the snap-through bifurcation is now a saddle-node/fold bifurcation.

the early stages and the under-damped oscillations about the natural state. The inset of Fig. 3 shows that the displacement of the midpoint initially grows quadratically in time, in contrast to the exponential growth that is observed in systems at the onset of instability [6, 16]; a systematic slowing down is also seen in both the displacement and the snap-through time, $t_{\rm snap}$ (inset of Fig. 4), as the bifurcation point $\Delta L_{\rm fold}$ is approached. This slowing down behaviour is reminiscent of critical slowing down in a number of physical phenomena [18–22].

To understand these observations, we analyse the linear beam equation, (1), incorporating the lateral confinement of the (inextensible) arch, which for small deflections is approximated by

$$\int_0^L \left(\frac{\partial w}{\partial x}\right)^2 \mathrm{d}x = 2\Delta L. \tag{3}$$

The inclination angle α enters through the boundary condition $w_x(0,t) = \alpha$ (subscripts denote differentiation) while the other boundary conditions are homogeneous, $w(0,t) = w(L,t) = w_x(L,t) = 0$. The linearity of the beam equation (1) and the form of the confinement (3) show that w_x can be rescaled by $(\Delta L/L)^{1/2}$ and, using L as the natural horizontal length scale, we see immediately that a single dimensionless parameter emerges:

$$\mu = \alpha \left(\frac{\Delta L}{L}\right)^{-1/2}. \tag{4}$$

The purely geometrical parameter μ is the key control parameter in the problem and may be understood as the ratio of the angle imposed by clamping, α, to that imposed by confinement, $(\Delta L/L)^{1/2}$.

An analysis of the equilibrium solutions of (1) subject to the constraint (3) and the appropriate boundary conditions allows the shape of the inverted arch to be determined analytically where it exists (see Supplementary Information for details). This analysis confirms that bistability of the inverted shape is lost at a saddle-node bifurcation where $\mu = \mu_{\rm fold} \approx 1.782$; the bifurcation shape, $w_{\rm fold}(x)$, and the associated (constant) compressive force, $PL^2/B = \tau_{\rm fold}^2 \approx 57.55$, can also be found explicitly.

To analyse the dynamics just beyond the bifurcation point, i.e. for end-shortenings ΔL slightly smaller than $\Delta L_{\rm fold}$, we set $\mu = \mu_{\rm fold} + \Delta\mu$ with $0 < \Delta\mu \ll 1$. Because no inverted equilibrium exists for $\Delta\mu > 0$, we exploit the fact that the midpoint displacement is initially the same as at the bifurcation, i.e. $w(L/2,0) = w_{\rm fold}(L/2)$. For small $\Delta\mu$, the initial shape of the strip is therefore 'close' to the bifurcation shape everywhere, $w(x,0) \approx w_{\rm fold}(x)$ for $0 < x < L$. Introducing dimensionless variables $X = x/L$, $W = w/(L\Delta L)^{1/2}$, $W_{\rm fold} = w_{\rm fold}/(L\Delta L)^{1/2}$, $\mathcal{T} = t/t_*$ and $\tau^2 = PL^2/B$ we then seek a series solution of the form

$$W(X,\mathcal{T}) = W_{\rm fold}(X) + \Delta\mu^{1/2} W_p(X) A(\mathcal{T}), \tag{5}$$

$$\tau(\mathcal{T}) = \tau_{\rm fold} + \Delta\mu^{1/2} A(\mathcal{T}). \tag{6}$$

We find that $W_p(X)$ is a spatial eigenfunction that can be determined analytically, while the temporal variation

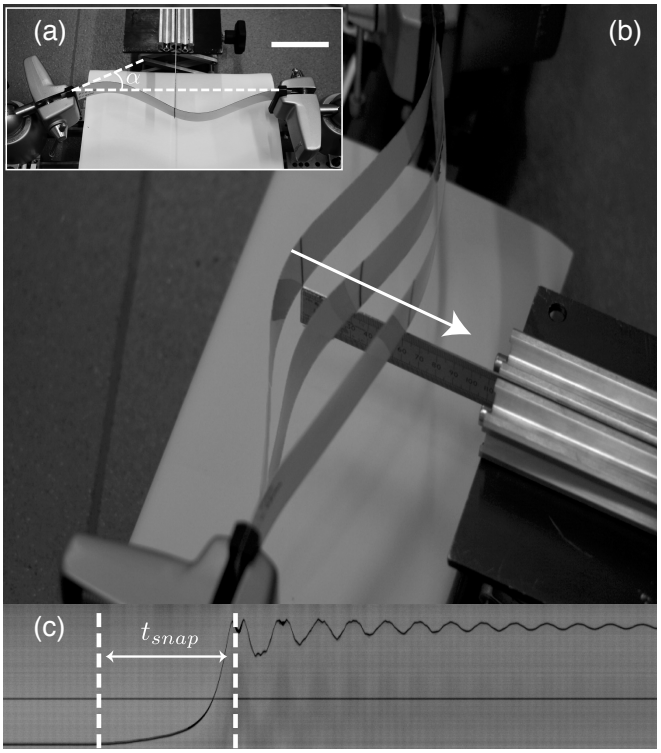

FIG. 2. Investigating the snapping dynamics of an elastic arch. (a) A thin strip is buckled into an unstable state with an end-shortening past the snapping transition, $\Delta L < \Delta L_{\rm fold}$; a metal indenter prevents the strip from snapping by making contact at its midpoint and imposes $w(L/2,0) = w_{\rm fold}(L/2)$. Scale bar 10 cm. (b) The indenter is then lowered allowing the arch to snap (three successive stages superimposed). (See also Methods and Supplementary Movie 1.) (c) A spatio-temporal plot of the midpoint reveals its trajectory during snapping (PET, $L = 240$ mm, $\alpha = 21.34°$, $\Delta L_{\rm fold} = 10.41$ mm, $w_{\rm fold}(L/2) = -16.75$ mm, $\Delta L = 10.20$ mm). The montage begins before the point when the indenter loses contact with the strip, and ends as the arch oscillates about the natural shape (the horizontal line is at zero displacement). Slices through a total of 828 frames (separated by 1 ms) are shown.

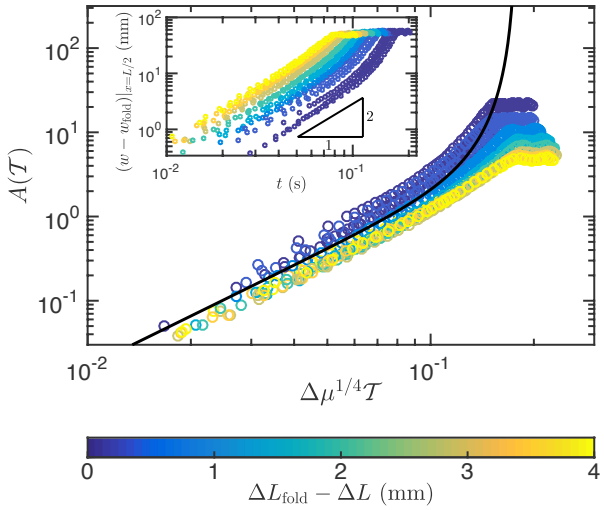

FIG. 3. Midpoint trajectories during snapping for different end-shortenings just beyond the snapping transition. Inset: Evolution of the midpoint position, $w(L/2,t)$, away from the initial value $w_{\rm fold}(L/2)$ (PET, $L = 290$ mm, $\alpha = 19.85°$, $\Delta L_{\rm fold} = 9.20$ mm, $w_{\rm fold}(L/2) = -20.95$ mm). For each value of $\Delta L_{\rm fold} - \Delta L$, three runs are recorded and shown here (circles). The time origin, $t = 0$, is the point where contact is first lost with the indenter (see Supplementary Information for details); data is plotted until the strip begins to oscillate about the natural shape. Main plot: The same data, rescaled in terms of the amplitude variable $A(\mathcal{T})$ as a function of dimensionless time $\mathcal{T} = t/t^*$. We see that while $A(\mathcal{T})$ remains small, the points collapse onto the predicted asymptotic behaviour (8) (solid black curve) with quadratic growth initially.

of the motion, $A(\mathcal{T})$, satisfies

$$\Delta\mu^{-1/2}\frac{{\rm d}^2A}{{\rm d}\mathcal{T}^2} = c_1 + c_2A^2, \tag{7}$$

with $c_1 \approx 329.0$ and $c_2 \approx 417.8$ constants that depend on $W_p(X)$ and its integrals (see Supplementary Information).

The ordinary differential equation (7) represents a great simplification of the full system (1) and (3). Furthermore, (7) is generic for the dynamics of elastic snap-through without dissipation: the nonlinear term A^2 is inherited from the structure of the saddle-node bifurcation (the parabolic geometry near the fold) and should hold generically in inertial snap-through. With viscous damping, a similar analysis would lead to a single time derivative in (7). The specific details of the problem (e.g. boundary conditions) enter only through the constants c_1 and c_2.

Because the arch starts from rest at a shape close to the bifurcation shape, the appropriate initial conditions for (7) are $A(0) = A_{\mathcal{T}}(0) = 0$, giving the implicit solution

$$\Delta\mu^{1/4}\mathcal{T} = \sqrt{\frac{3}{2}}\int_0^{A(\mathcal{T})}\frac{{\rm d}\xi}{(3c_1\xi + c_2\xi^3)^{1/2}}. \tag{8}$$

Expanding the right-hand side for $A \ll 1$, we obtain the asymptotic behaviour

$$A(\mathcal{T}) \sim \frac{c_1}{2}\Delta\mu^{1/2}\mathcal{T}^2,$$

when $\mathcal{T} \ll \Delta\mu^{-1/4}$. The initial growth of the midpoint displacement (and all other material points) is therefore ballistic, as observed experimentally (Fig. 3 inset); viscous dissipation would instead give $A \propto \mathcal{T}$. Furthermore, the full solution for $A(\mathcal{T})$ computed from (8) compares favourably to that observed experimentally while $A \lesssim 1$ (Fig. 3), with experimental data for different values of $\Delta\mu$ collapsing onto a single master curve. For $A \gg 1$ our asymptotic analysis breaks down and fails to predict how the strip approaches the natural equilibrium and oscillates; instead, the solution (8) blows up at time $\mathcal{T} = \mathcal{T}_{\rm b}$

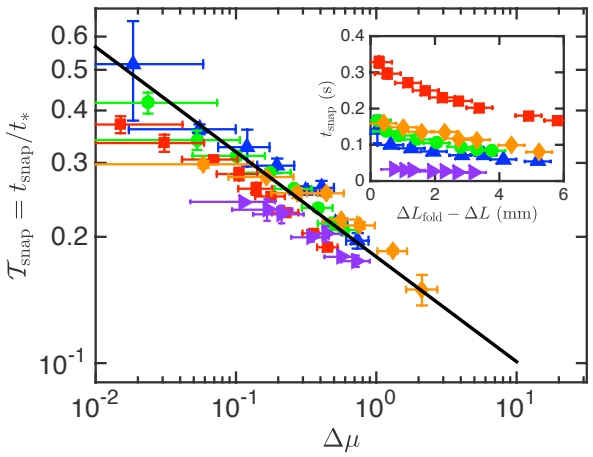

FIG. 4. Slowing down of snapping dynamics near the loss of bistability. Inset: The experimentally measured snapping time, $t_{\rm snap}$ (defined as the time taken to reach the first peak of vibrations, as labelled in Fig. 2c, averaged over three runs), as the end-shortening ΔL approaches the snapping threshold $\Delta L_{\rm fold}$ from below. Data is shown for PET strips with $L = 240$ mm, $\alpha = 21.34°$ (upward-pointing triangles), $L = 290$ mm, $\alpha = 19.85°$ (circles) and $L = 430$ mm, $\alpha = 21.17°$ (squares), as well as for experiments on steel strips with $L = 140$ mm, $\alpha = 22.51°$ (right-pointing triangles) and 280 mm, $\alpha = 17.14°$ (diamonds). Main plot: Snapping times, re-scaled by the inertial timescale t^*, as a function of the normalized distance to bifurcation $\Delta\mu = \mu - \mu_{\rm fold}$ (computed from (4)). The data collapse onto the asymptotic prediction $\mathcal{T}_{\rm snap} \approx 0.179\Delta\mu^{-1/4}$ from linear beam theory (solid black line). Horizontal error bars correspond to the uncertainties in measurements of α ($\pm 2°$) and ΔL (± 200 μm) (see Methods); vertical error bars correspond to the standard deviation of the measured snapping times over three runs.

where

$$\mathcal{T}_{\rm b} = \sqrt{\frac{3}{2}}\Delta\mu^{-1/4}\int_0^\infty \frac{{\rm d}\xi}{(3c_1\xi + c_2\xi^3)^{1/2}} \approx 0.179\Delta\mu^{-1/4}. \tag{9}$$

This time therefore corresponds to the end of the 'bottleneck phase' in which the strip is influenced by its proximity to the inverted equilibrium at the fold. Because the motions are rapid by this stage, $\mathcal{T}_{\rm b}$ represents a natural approximation for the total snap-through time. The prediction (9) leads to a collapse of experimentally measured snapping times for strips composed of different materials and natural lengths L, and predicts the dependence on $\Delta\mu$ well (Fig. 4).

The data in Fig. 4 and the expression for the snap-through time, (9), show that as the system approaches the snap-through transition the dynamics slow down significantly. This is characteristic of the dynamics near a bifurcation in a range of physical phenomena [19–23], which is commonly referred to as 'critical slowing down' [18], or as a 'bottleneck' due to the 'ghost' of the nearby equilibrium [24]. The importance of critical slowing down in elastic instabilities such as snap-through has not been appreciated previously, despite numerous previous experiments showing signs of diverging time scales as the threshold is approached [13, 14]. Furthermore, the inertial (rather than overdamped) dynamics here changes the exponents typically seen in critical slowing down ($\Delta\mu^{-1/4}$ rather than $\Delta\mu^{-1/2}$ [23]).

We note that the prefactor in the scaling $\mathcal{T}_{\rm b} \sim \Delta\mu^{-1/4}$ depended on a detailed calculation and hence on the boundary conditions of the problem; here the prefactor is small, meaning that the snap-through time is comparable to the characteristic elastic time scale t_* for experimentally attainable $\Delta\mu$. However, in other systems the appropriate prefactor may be substantially larger and finer control of the distance to bifurcation $\Delta\mu$ may be possible; in such circumstances we expect that a substantial disparity between the observed snap-through time and the characteristic elastic time scale t_* may emerge. Biological systems such as the Venus flytrap may be particularly prone to such a slowing down, as the analogue of $\Delta\mu$ is often controlled by slow processes such as swelling or growth. In both biological and engineering settings, snap-through would seem to require a trade-off between the speed of snapping (a faster snap requiring larger $\Delta\mu$) and the time/energy taken to attain a large $\Delta\mu$. Critical slowing down may also mean that very close to the snap-through transition the system becomes overdamped (rather than inertial) leading to different scalings and slower dynamics; this possibility remains to be fully explored and may depend on the precise nature of the damping present (e.g. viscoelasticity in man-made applications [14] or poroelasticity in biological systems [7, 9]). Our analysis, combined with techniques for controlling snap-through such as solvent-induced swelling [25] or photo-initiation [26], may offer the possibility to tune the time scale of snap-through from fast to slow by controlling how far beyond the transition one takes the system.

[1] Bazant, Z. & Cendolin, L. *Stability of Structures: Elastic, Inelastic, Fracture, and Damage Theories* (Oxford University Press, 1991).

[2] Loh, O. Y. & Espinosa, H. D. Nanoelectromechanical contact switches. *Nature Nanotech.* **7**, 283–295 (2012).

[3] Xu, P. *et al.* Unusual ultra-low-frequency fluctuations in freestanding graphene. *Nature Comm.* **5**, 3720 (2014).

[4] Silverberg, J. L. *et al.* Origami structures with a critical transition to bistability arising from hidden degrees of freedom. *Nature Mat.* **14**, 389–393 (2015).

[5] Dudte, L. H., Vouga, E., Tachi, T. & Mahadevan, L. Programming curvature using origami tessellations. *Nature Mater.* **15**, 583–588 (2016).

[6] Pandey, A., Moulton, D. E., Vella, D. & Holmes, D. P.

Dynamics of snapping beams and jumping poppers. *EPL* **105**, 24001 (2014).
[7] Skotheim, J. M. & Mahadevan, L. Physical limits and design principles for plant and fungal movements. *Science* **308**, 1309–1310 (2005).
[8] Forterre, Y. Slow, fast and furious: understanding the physics of plant movements. *J. Exp. Bio.* **64**, 4745–4760 (2013).
[9] Forterre, Y., Skotheim, J. M., Dumais, J. & Mahadevan, L. How the Venus flytrap snaps. *Nature* **433**, 421–425 (2005).
[10] Smith, M. L., Yanega, G. M. & Ruina, A. Elastic instability model of rapid beak closure in hummingbirds. *J. Theo. Bio.* **282**, 41–51 (2011).
[11] Gonçalves, P. B. *et al.* Dynamic non-linear behavior and stability of a ventricular assist device. *Int. J. Solids Struct.* **40**, 5017–5035 (2003).
[12] Daynes, S., Potter, K. & Weaver, P. M. Bistable prestressed buckled laminates. *Comp. Sci. Tech.* **68**, 3431–3437 (2010).
[13] Hung, E. S. & Senturia, S. D. Generating efficient dynamical models for microelectromechanical systems from a few finite-element simulation runs. *J. MEMS* **8**, 280–289 (1999).
[14] Brinkmeyer, A., Pirrera, A., Santer, M. & Weaver, P. M. Pseudo-bistable pre-stressed morphing composite panels. *Int. J. Solids Struct.* **50**, 1033–1043 (2013).
[15] Plaut, R. H. & Virgin, L. N. Vibration and snap-through of bent elastica strips subjected to end rotations. *J. Appl. Mech.* **76**, 041011 (2009).
[16] Fargette, A., Neukirch, S. & Antkowiak, A. Elastocapillary snapping: capillarity induces snap-through instabilities in small elastic beams. *Phys. Rev. Lett.* **112**, 137802 (2014).
[17] Pippard, A. B. *Response and Stability* (Cambridge University Press, 1985).
[18] Chaikin, P. M. & Lubensky, T. C. *Principles of Condensed Matter Physics* (Cambridge University Press, 2000).
[19] Tredicce, J. R. *et al.* Critical slowing down at a bifurcation. *Am. J. Phys.* **72**, 799–809 (2004).
[20] Strogatz, S. H. & Westervelt, R. M. Predicted power laws for delayed switching of charge-density waves. *Phys. Rev. B* **40**, 10501 (1989).
[21] Dakos, V. *et al.* Slowing down as an early warning signal for abrupt climate change. *Proc. Natl Acad. Sci.* **105**, 14308–14312 (2008).
[22] Scheffer, M. *et al.* Early-warning signals for critical transitions. *Nature* **461**, 53–59 (2009).
[23] Aranson, I. S., Malomed, B. A., Pismen, L. M. & Tsimring, L. S. Crystallization kinetics and self-induced pinning in cellular patterns. *Phys. Rev. E* **62**, R5–R8 (2000).
[24] Strogatz, S. H. *Nonlinear Dynamics and Chaos with Applications to Physics, Biology, Chemistry and Engineering* (Westview Press, Philadelphia, 2015).
[25] Holmes, D. P. & Crosby, A. J. Snapping surfaces. *Adv. Mater.* **19**, 3589–3593 (2007).
[26] Shankar, M. R. *et al.* Contactless, photoinitiated snap-through in azobenzene-functionalized polymers. *Proc. Natl. Acad. Sci.* **110**, 18792–18797 (2013).

ACKNOWLEDGMENTS

We are grateful to Jean-Baptiste Gorce for early experiments in a related system and to Jonathan Dawes, Sébastien Neukirch, and Jin-Chong Tan for discussions. The research leading to these results has received funding from the European Research Council under the European Union's Horizon 2020 Programme / ERC Grant Agreement no. 637334 (DV) and the EPSRC (MG).

AUTHOR CONTRIBUTIONS

DV designed the research. MG performed experiments. MG, DEM and DV performed the analysis and wrote the paper.

COMPETING FINANCIAL INTERESTS

The authors declare no competing financial interests.

METHODS

Sample preparation. Strips were prepared from biaxially oriented polyethylene terephthalate (PET) film (Goodfellow, Cambridge, $\rho_s = 1.337\,\mathrm{g\,cm^{-3}}$, $h = 0.35$ mm, $E = 5.707$ GPa) and stainless steel rolled shim (304 grade, RS components, $\rho_s = 7.881\,\mathrm{g\,cm^{-3}}$, $h = 0.1$ mm, $E = 203.8$ GPa). The values of the Young's modulus E were determined by analysing the frequency of small-amplitude vibrations of the strip. The time scale of snapping was varied by varying the length of the strip: for PET we used lengths $L \in \{240, 290, 430\}$ mm while for steel we used $L \in \{140, 280\}$ mm.

Snapping experiments. The ends of each strip are clamped into vice clamps (PanaVise 301) which are mounted onto a linear track so that the strip deforms in one plane only. To minimize the effect of gravity, the strip is oriented sideways so its width lies in the vertical direction (see Fig. 2a,b of the main text). The right clamp is fixed parallel to the track, while the left clamp holds the strip at an angle $\alpha \neq 0$ (constant throughout each experiment) and can be moved along the track to vary the applied end-shortening ΔL. A digital camera mounted above the left clamp allows α to be determined to an accuracy of $\pm 2^\circ$, and changes in ΔL to be measured to an accuracy of ± 200 μm (by measuring displacement of the clamp from a known reference state).

The snapping dynamics are filmed using a high speed camera (Phantom Miro 310) at a frame rate of 1000 fps. The camera is placed vertically above the strip, allowing the midpoint position (marked on the edge) to be recorded when the strip is in equilibrium and during motion. Beyond the fold, i.e. when only one equilibrium exists, the strip is forced to start close to the fold shape using a metal ruler (tip width 1 mm) attached to a laboratory jack; this is then lowered vertically out of contact with the strip to allow snapping to proceed. The resulting movie is cropped around the midpoint position and converted to a spatio-temporal plot (montage) of its trajectory using ImageJ (NIH).

Data availability. The experimental data that supports the plots within this paper and other findings of this study are available from doi `10.5287/bodleian:RyGXnqJGk`.

[1] Bazant, Z. & Cendolin, L. *Stability of Structures: Elastic, Inelastic, Fracture, and Damage Theories* (Oxford University Press, 1991).